

An Atom and a Photon

J. Volz^{a,*}, M. Weber^a, D. Schlenk^a, W. Rosenfeld^a, C. Kurtsiefer^b, and H. Weinfurter^{a,c,**}

^a *Department für Physik, Ludwig-Maximilians-Universität München, München, D-80799 Germany*

^b *Department of Physics, National University of Singapore, Singapore*

^c *Max-Planck-Institut für Quantenoptik, Garching, 85748 Germany*

*e-mail: volz@lmu.de

**e-mail: h.w.@lmu.de

Received January 12, 2007

Abstract—The coherent control of single-photon emitters as, e.g., single ions or atoms, is a crucial element for mapping quantum information between light and matter. The possibility of generating entanglement between a photon and the emitter system provides an interface between matter-based quantum memories and photonic quantum communication channels, which is the essential resource for quantum repeaters and other future quantum information applications. To generate entangled atom–photon states, in our experiment, we store a single ⁸⁷Rb atom in an optical dipole trap. The single-atom/single-photon character is confirmed by the observation of photon antibunching in the detected fluorescence light. The spectral properties of single photons emitted by the atom allowed us to determine the mean kinetic energy of the atom corresponding to 105 μ K. We describe a single-atom state analysis method which allowed us to characterize the entanglement between the atom and a single photon emitted in the spontaneous decay. We obtain an entanglement fidelity of 89% that clearly shows the high degree of entanglement in our system and potential for further applications in quantum communication.

PACS numbers: 03.67.-a, 32.80.Qk, 42.50.Ar, 42.50.Xa

DOI: 10.1134/S1054660X0707016X

1. INTRODUCTION

Interaction of light with trapped ions was one of the many fields where Herbert Walther and his team made decisive contributions, such as the observation of non-classical light emitted from a single ion [1], the observation of subnatural line widths [2], or the coherent control of ions interacting with cavity fields [3], to name just a few. This paper, dedicated to the memory of Herbert Walther, describes experiments on the entanglement between an atom and a photon, where we could “discover” several such features of trapped atoms—of course, many of them were already demonstrated in his initial experiments on single ions.

Cold atoms share several properties with trapped ions, which make them well suited for experiments on the foundations of quantum mechanics and quantum optics. On the one hand, narrowband atomic transitions enable the controlled generation of single photons. On the other hand, the well-defined internal level structure makes atoms also an ideal choice for the realization of long-lived quantum memories. Compared to ions, the wavelengths for manipulating the transitions, as well as the ones of the fluorescence light, are, particularly in the case of rubidium, accessible with laser diodes and efficiently detectable with single-photon avalanche photo diode. In turn, such simplifications enable one to increase the complexity of the experimental procedures and to demonstrate new features of light interacting with matter.

In this contribution, we describe experiments with a single laser-cooled ⁸⁷Rb atom, localized in a far-off resonant optical dipole trap (FORT) [4, 5]. The level structure of the atomic ground state $5^2S_{1/2}$ is well suited as quantum memory due to the very small relaxation rate [6]. The stored quantum information can, in principle, be converted to communication qubits, i.e., to photons at a wavelength of 780 nm, and, therefore, can be easily transmitted between specified remote locations. And, most importantly, the spontaneous decay of a single ⁸⁷Rb atom prepared in the $5^2P_{3/2}, F' = 0$ excited-state hyperfine level can be used to generate entanglement between the spin state of the atom and the polarization of the emitted photon [7, 8] making this system an essential component for the implementation of future quantum communication methods [9].

Here, we report on the observation and analysis of a single ⁸⁷Rb atom in an optical dipole trap that operates at a detuning of 61 nm, i.e., 4.5×10^6 line widths from atomic resonance. Atoms stored in this FORT have a very low photon scattering rate and, therefore, negligible photon recoil heating. Confinement times of 4 s, limited only by background gas, are achieved with no additional cooling. Because of the small trap volume, only a single atom is loaded at a time [10]. To prove this property, the photon statistics of the detected fluorescence light has been studied with a Hanbury–Brown–Twiss (HBT) setup. The measured second-order corre-

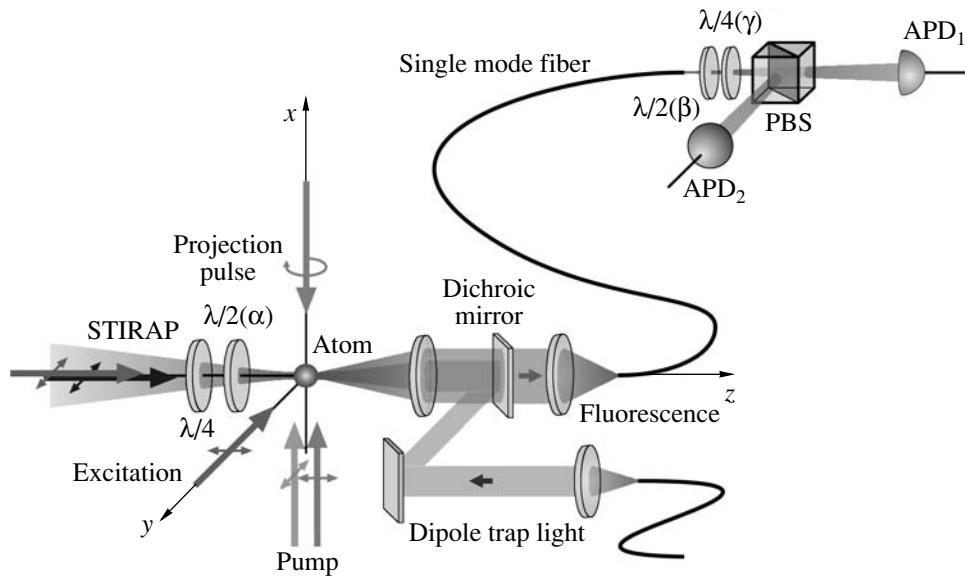


Fig. 1. Experimental setup for the observation of single trapped atoms and for the generation and analysis of atom–photon entanglement. The atom is loaded from a MOT (beams and coils not shown) into the dipole trap focused to a waist of $3.5\ \mu\text{m}$. Single-photon fluorescence from the atom is collected in a confocal setup, separated from the dipole trap beam by a dichroic mirror and guided to single-photon detectors or a cavity to measure the atom’s temperature. For the observation of entanglement between the atom and the emitted photon, first, optical pumping into the $F = 1, m_F = 0$ Zeeman sublevel and a subsequent excitation prepares the atom in the excited hyperfine level $5\ ^2P_{3/2}, F' = 0$. In the following spontaneous decay, entanglement between the polarization of the emitted photon and the magnetic quantum number of the atom is created. The emitted photon is coupled into a single-mode optical fiber and registered in a single-photon polarization analyzer. After photon detection, the STIRAP pulse sequence transfers a certain superposition of Zeeman sublevels to the $F = 2$ hyperfine ground level of the atom, followed by hyperfine level detection (Fig. 5).

lation function exhibits strong photon antibunching verifying that, indeed, only a single atom is present in the trap. Similar to the effects observed in the initial experiments with trapped ions [1], the two-photon correlations show coherent dynamics of the population of the atomic hyperfine levels involved in the excitation process. Yet, here, the observed correlations cannot be explained by the simple model of a two-level atom [11]. In order to simulate the second-order correlation function of the measured fluorescence light, we numerically solve optical Bloch equations based on a four-level model. Within experimental errors, we find good agreement of the theoretical predictions with the experimental data. Furthermore, we analyzed the spectral properties of the emitted single photons with a scanning Fabry–Perot interferometer (FPI). Due to the Doppler effect, we observe a broadening of the Rayleigh scattered atomic fluorescence spectrum relative to the spectral distribution of the exciting laser light field. This broadening allows us to determine the mean kinetic energy of the trapped atom corresponding to a temperature of $105\ \mu\text{K}$. Finally, after developing a single-atom state analysis, we were able to observe and to characterize entanglement between the internal state of a single atom and the polarization state of the emitted photon.

2. EXPERIMENTAL SETUP

In our experiment, the FORT is generated by a Gaussian laser beam of a single-mode laser diode at a wavelength of $856\ \text{nm}$, which is focused with a microscope objective (located outside the vacuum chamber) to a waist of $3.5 \pm 0.2\ \mu\text{m}$ (see Fig. 1). For a laser power of $44\ \text{mW}$, we calculate a trap depth of $1\ \text{mK}$ and a photon scattering rate of $24\ \text{s}^{-1}$ [12]. In order to load atoms into this FORT, we start with a cloud of laser-cooled atoms in a magneto-optical trap (MOT) [13]. The MOT is loaded from the thermal rubidium background gas produced by a dispenser operating slightly above threshold (residual gas pressure below $10^{-10}\ \text{mbar}$). This provides a macroscopic reservoir of cold atoms with a typical temperature on the order of $100\ \mu\text{K}$. The dipole trap overlaps with the MOT and, thus, by changing the magnetic field gradient of the MOT, we can adjust the loading rate of atoms into the dipole trap between $0.2\ \text{s}^{-1}$ without the quadrupole field, and $1\ \text{atom per second}$ at a magnetic field gradient of $1\ \text{G/cm}$. To assure optimal conditions for laser cooling in the dipole trap, the magnetic field is compensated below a residual value of $300\ \text{mG}$ by three orthogonal pairs of Helmholtz coils generating a suitable bias field.

The fluorescence light scattered by atoms in the dipole trap region is collected with the focusing objec-

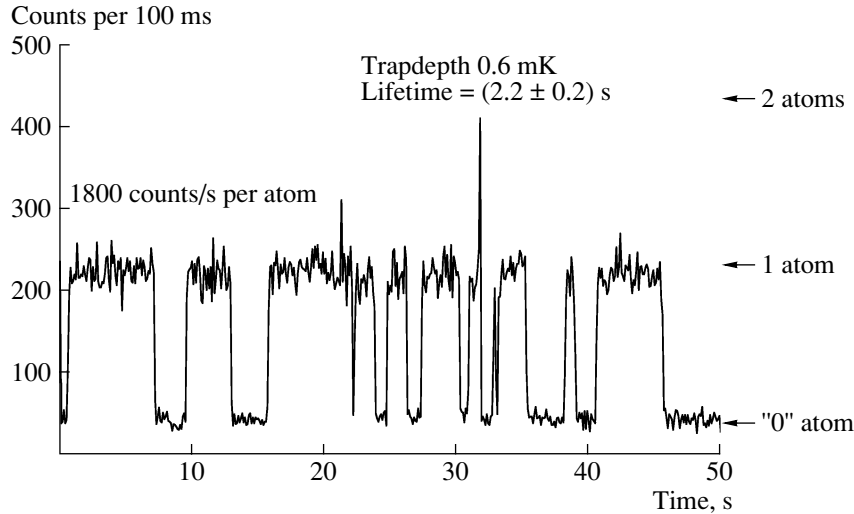


Fig. 2. Single-atom detection. The plot shows the number of photons counted by the Si APD when atoms are loaded into the dipole trap. With an average of 1800 additional counts/s, single atoms in the trap can be clearly discriminated against background (450 counts/s). Two atoms in the trap are lost immediately due to collisional blockade.

tive, and, in a confocal configuration, separated from the trapping beam with a dichroic mirror. Then, it is coupled into a single-mode optical fiber for spatial filtering and detected with a Si avalanche photodiode (APD). In this way, it is possible to suppress stray light from secular reflections of the cooling beams and fluorescence light from atoms outside the dipole trap.

To load a single atom into the FORT, first cooling and repump lasers of the MOT are switched on and the fluorescence count rate from the dipole trap is observed. If a cold atom enters the trap, the detected fluorescence count rate increases significantly and indicates the presence of the atom. Typically, we observe an additional photon count rate of 500–1800 s^{-1} per atom, depending on the detuning and intensity of the cooling laser. From the overlap of the detection beam (waist, $2.2 \pm 0.2 \mu\text{m}$) with the emission characteristics of the emitted atomic fluorescence, we calculate an overall detection efficiency for single photons of 0.1% including transmission losses and the quantum efficiency of our Si APD.

The fluorescence rate exhibits the typical telegraph-signal structure (see Fig. 2) jumping between background intensity (450 s^{-1}) when no atom is in the trap and a defined intensity level (2250 s^{-1}) corresponding to one atom. Fluorescence from more than one atom in the trap was hardly observed. This is due to light-induced two-body collisions [14], which for the small trap volume, give rise to a blockade mechanism. This assures that only a single atom is trapped per time. If a second atom enters the trap, these collisions lead to an immediate loss of both atoms [10].

Whereas in single-ion experiments a random telegraph signal originates from transitions to shelving states [15], here it occurs since a single atom enters and

leaves the much shallower trap. Thus, from the fluorescence trace in Fig. 2, we can determine the $1/e$ lifetime in the presence of cooling light to be $2.2 \pm 0.2 \text{ s}$. The cooling light is only necessary to load the trap; thereafter, it can also reduce the atomic lifetime due to light induced two-body collisions. Thus, the mean lifetime without cooling light is significantly longer, about $4.4 \pm 0.2 \text{ s}$. Due to the interaction with the far-off resonant dipole trap laser field, spontaneous Raman scattering leads to a change of the population occupation of an atom initially pumped to the $F = 1$ hyperfine ground level. This hyperfine state changing scattering rate was determined in a measurement, similar to [6], to 0.1 s^{-1} for a trap depth of 0.75 mK.

3. PHOTON STATISTICS

To assure that the upper fluorescence level corresponds to a single trapped atom, we analyzed the non-classical properties of the emitted fluorescence light. For this purpose, the second-order correlation function $g^{(2)}(\tau)$ was measured in a Hanbury–Brown–Twiss configuration with two detectors behind a 50 : 50 beam splitter. The differences in detection times $\tau = t_1 - t_2$ of photon pair events were recorded in a storage oscilloscope with a conditional trigger mode. To minimize background contributions, the coincidences are acquired only at times when the fluorescence exceeded a threshold of 1200 counts/s.

A normalized distribution of time differences τ is equivalent to the second-order correlation function as long as τ is much smaller than the mean time difference between two detection events [16]. For correct normalization of the measured $g^{(2)}(\tau)$, we divide the coincidences in each time bin $\Delta\tau$ by $r_1 r_2 \Delta\tau T$, where r_1 and r_2

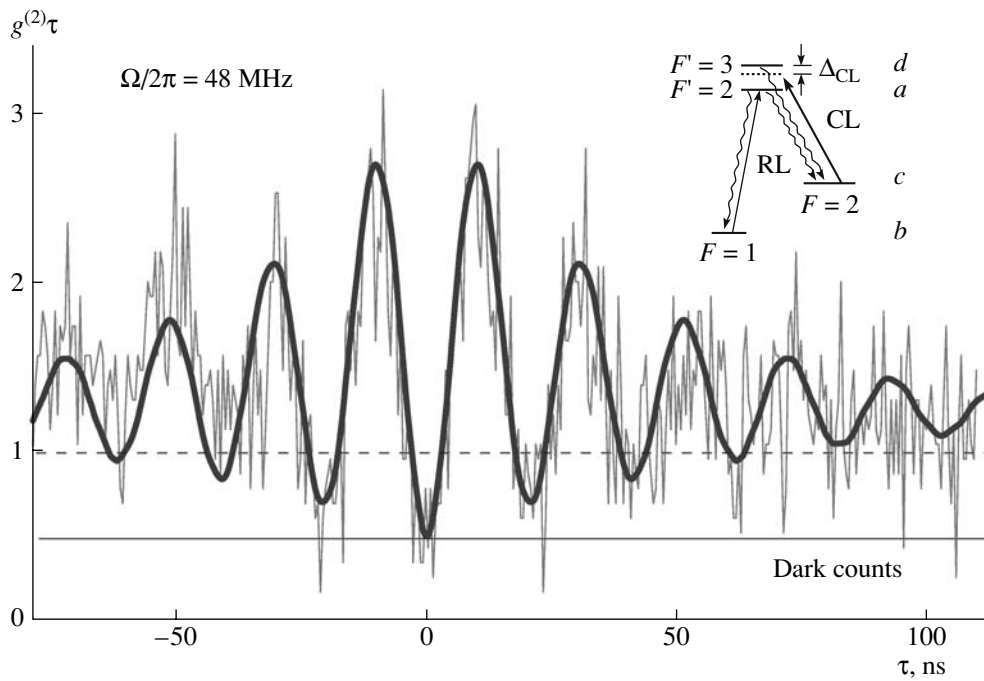


Fig. 3. Intensity correlation function $g^{(2)}(\tau)$ of the resonance fluorescence from a single ^{87}Rb atom. Thin line: measured correlation function. Bold line: numerical calculation according to the four-level structure shown in the inset. Experimental parameters: $I_{\text{CL}} = 103 \text{ mW/cm}^2$, $I_{\text{RL}} = 12 \text{ mW/cm}^2$, $\Delta_{\text{CL}}/2\pi = -31 \text{ MHz}$, dipole trap depth $U = 0.38 \text{ mK}$.

are the mean count rates of the two detectors, and T is the total measurement time with an atom in the trap.

The resulting pair correlation function $g^{(2)}(\tau)$ for trap depth $U = 0.38 \pm 0.04 \text{ mK}$, cooling laser intensity $I_{\text{CL}} \approx 103 \text{ mW/cm}^2$, and detuning $\Delta_{\text{CL}}/2\pi$ of -31 MHz is shown in Fig. 3. We observe an uncorrected minimum value $g^{(2)}(0) = 0.52 \pm 0.14$ at zero delay ($\tau = 0$). Taking into account accidental coincidences due to the dark count rate of 300 s^{-1} of each detector, we derive a corrected minimum value $g_{\text{corr}}^{(2)}(0) = 0.02 \pm 0.14$. Within our experimental errors, this is compatible with perfect photon antibunching of the emitted fluorescence light and, therefore, proves the single-atom character of our dipole trap. Furthermore, we observe the signature of Rabi oscillations due to the coherent interaction of the cooling and repump laser field with the atomic hyperfine levels involved in the excitation process. The oscillation frequency is in good agreement with a simple two-level model [11] and the amplitude is damped out on the expected time scale of the $5^2P_{3/2}$ excited-state lifetime (27 ns).

The correlation function of a driven two-level atom shows its maximum value $g_{\text{max}}^{(2)} = 2$ for τ close to zero [11]. In contrast, the correlations observed here show, after background correction, larger oscillation amplitudes up to a maximum value of 5! This increase of the oscillation amplitude—already known from experiments with single ions [17]—is a consequence of opti-

cal pumping among the two hyperfine ground levels $F = 1$ and 2 . To understand the consequences of this effect on the second-order correlation function in detail, one has to take into account the structure of all atomic levels involved in the cooling and fluorescence process.

In our experiment, we use the MOT cooling laser (CL), red detuned to the unperturbed hyperfine transition $5^2S_{1/2}, F = 2 \rightarrow 5^2P_{3/2}, F' = 3$ (inset of Fig. 3) by $\Delta_{\text{CL}} = -5\Gamma$ ($\Gamma = 2\pi \times 6 \text{ MHz}$ is the natural line width) for the observation of fluorescence. To avoid optical pumping to the $5^2S_{1/2}, F = 1$ hyperfine ground level, we additionally shine in a repump laser (RL) on resonance with the unperturbed hyperfine transition $5^2S_{1/2}, F = 1 \rightarrow 5^2P_{3/2}, F' = 2$. The significant population in $F = 1$ leads to the breakdown of the two-level assumption, and the atomic system must be approximated by an effective four-level system [18].

For the following calculation, we, first, simplify the internal atomic dynamics by neglecting the Zeeman substructure of the involved hyperfine levels, and, second, treat the exciting cooling and repump light fields as unpolarized with an average intensity of six times the single beam intensity I . From the numerical solutions of the equation of motion for the atomic density matrix of a four-level system, we calculate $g^{(2)}(\tau)$ with the help of the quantum regression theorem [19], which relates the two-time expectation values of the correlation function to particular one-time expectation

values and the initial conditions for the density matrix ρ [20]. As we do not distinguish from which hyperfine transition the first photon of a pair event came from, the initial condition for $\rho(t=0)$ for the numerical solution was calculated from the steady-state solution $\rho(t=\infty)$. The resulting correlation function is, then, given by the ratio of the excited state populations at time τ and in the steady state ($t=\infty$)

$$g^{(2)}(\tau) = \frac{\rho_{aa}(\tau) + \rho_{dd}(\tau)}{\rho_{aa}(\infty) + \rho_{dd}(\infty)}. \quad (1)$$

Here, ρ_{ss} indicates the population of level s (see Fig. 3, inset). For our experimental parameters, we calculated the second-order correlation in (1) following the described procedure. Figure 3 shows the measured uncorrected correlation function and the result of the numerical simulation of the optical Bloch equations. Increasing the dipole trap depth U from 0.38 to 0.81 mK without changing the laser cooling parameters enlarges the effective detuning of the cooling laser to the hyperfine transition $5^2S_{1/2}, F=2 \rightarrow 5^2P_{3/2}, F'=3$ due to an increase in the ac Stark shift of the respective atomic levels in the far-off resonant dipole-trap laser field. This effect gives rise to an increase in the effective Rabi frequency from 47.5 to 62.5 MHz [18].

To summarize, within our experimental errors we find good agreement of the calculated second-order correlation function with the measured correlations. Due to the more complex excitation scheme, a four-level model is required to correctly describe the observed oscillation amplitude of the second-order correlation function. Within experimental errors, we observe perfect photon antibunching, which proves that only a single atom is present in our dipole trap.

4. SPECTRAL PROPERTIES—TEMPERATURE OF THE SINGLE ATOM

In the present experiment, a single optically trapped atom is cooled by three-dimensional polarization gradients in an optical molasses. This should lead to a final kinetic energy on the order of 100 μ K [21]. Due to the motion of the atom in the confining potential, the Doppler effect causes a line broadening in the emitted fluorescence spectrum. Hence, a spectral analysis of the atomic resonance fluorescence yields information about the kinetic energy of the trapped atom.

For low excitation intensities, the fluorescence spectrum of a two-level atom exhibits an elastic peak centered at incident laser frequency ω_L , while, for higher intensities, an inelastic component becomes dominant, with contributions at frequencies ω_L and $\omega_L \pm \Omega_0$ [22], where Ω_0 denotes the effective Rabi frequency. This so-called ‘‘Mollow triplet’’ arises from the dynamical Stark splitting of the two-level transition and has been observed in a number of experiments, using low-density atomic beams [23, 24] or a single trapped and laser-cooled Ba⁺ ion [25]. Surprisingly, there are only few

experimental investigations of the elastic scattering process with a frequency distribution of the resonance fluorescence equal to the exciting laser. Subnatural line widths were demonstrated with atomic beam experiments [24, 26], atomic clouds in optical molasses [27], and in Herbert Walther’s group with a single trapped and laser-cooled Mg⁺ ion [2].

For our laser cooling parameters, the fluorescence spectrum is dominated by elastic Rayleigh scattering [20, 22]. Hence, the emitted fluorescence light exhibits the frequency distribution of the exciting laser field (0.6 MHz FWHM) broadened by the Doppler effect. Position-dependent atomic transition frequencies in the dipole trap, due to the inhomogeneous ac Stark shift (caused by the finite kinetic energy), give no additional broadening, because the spectrum of the elastically scattered fluorescence light is determined only by the frequency distribution of the exciting light field and not by the atomic transition frequencies.

The spectrum of the single photons emitted in the scattering process is analyzed with a scanning Fabry–Perot interferometer (FPI) with a frequency resolution of 0.45 MHz (FWHM), a transmission of 40%, and a finesse of 370. To measure the spectrum only at times when a single atom is present, a part of the fluorescence light is monitored separately with a reference APD (APD₁ in Fig. 4). Since the broadening of the atomic emission spectrum due to the Doppler effect is small, the instrumental function of the spectrometer and the exciting laser line width have to be known accurately. In order to achieve this, we shine a fraction of the exciting light (reference beam) into the collection optics (see Fig. 4). This way, both reference and scattered light are subject to the identical spectrometer instrumental function, whereby the reference laser spectrum is also used to monitor length drifts of the analyzing cavity. In the experiment, the spectrum of the reference beam and the fluorescence light scattered by the atom were recorded alternately. After each measurement, a compensation of the cavity length drift was performed by referencing the cavity frequency to the point of maximum transmission of the reference laser.

With this procedure, we obtained the two (normalized) data sets in Fig. 4. As expected, the resonance fluorescence spectrum exhibits a ‘‘subnatural’’ line width of 1.00 ± 0.02 MHz (FWHM), because the elastic Rayleigh contribution dominates the scattering process. The exciting laser light field exhibits a line width of 0.90 ± 0.02 MHz (FWHM), which is the convolution of the transmission function of the Fabry–Perot resonator with the spectral width of the excitation laser. The depicted error bars reflect the statistical error from the individual count rates of each data point. For the reference laser spectrum, this error is too small to be visible in this graph.

For an atom at rest, the resonance fluorescence spectrum shows the same line width as the exciting light field. Any finite kinetic energy distribution of the atom

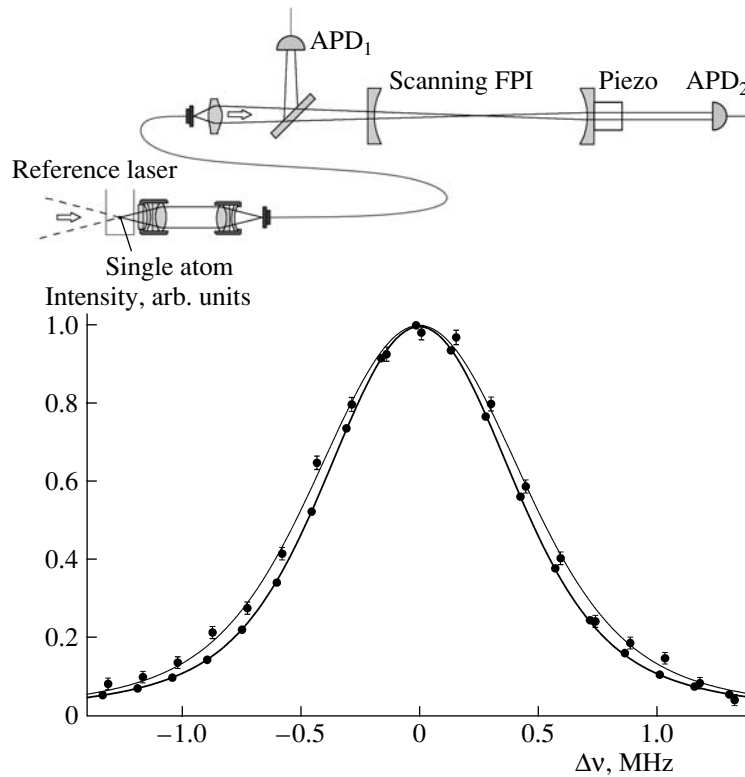


Fig. 4. Setup for the measurement of the resonance fluorescence spectrum of light scattered by a single ^{87}Rb atom. Both the atomic fluorescence and the laser light are analyzed alternately with the same scanning FPI. The spectra exhibit a width of 0.90 ± 0.02 MHz and 1.00 ± 0.02 MHz (FWHM) for excitation (blue) and fluorescence light (red), respectively.

will lead to a broadening of the atomic emission spectrum and, therefore, can be used for the determination of the atomic “temperature.” To extract the mean kinetic energy from the measured spectra in Fig. 4, we assume that the atom is subject to the same stationary Gaussian velocity distribution in all directions. This assumption is justified, because the atom is expected to occupy on average up to 100 motional states of the dipole trap potential [21]. Therefore, the atomic motion can be considered classical and the energy distribution is given by the Boltzmann statistics, leading to a thermal velocity distribution. Fitting a Gaussian profile convolved with the reference laser line profile, we directly obtain the mean kinetic energy $E_{\text{kin}} = (105 \pm 24)_{-17}^{+14} \mu\text{K} \times k_B$ of the single atom in the dipole trap. Within the experimental errors, the measured temperature is equal to or smaller than the Doppler temperature of ^{87}Rb ($146 \mu\text{K}$).

5. SINGLE-ATOM STATE ANALYSIS

Having quantum information applications or other spin-1/2 experiments in mind, we first have to define an atomic qubit state. The qubit, here, can be represented by the two Zeeman sublevels $|1, -1\rangle$ and $|1, +1\rangle$, and the goal now is to analyze any superposition of these two

states. In our experiment, the atomic state measurement is realized using a combination of coherent dark state projection together with a population transfer between the two hyperfine ground levels of ^{87}Rb . Therefore, we make use of the so-called stimulated Raman adiabatic passage (STIRAP) technique that allows coherent population transfer between atomic levels by an adiabatic change of the intensity of the involved light fields [28]. To analyze superpositions of Zeeman sublevels, we employ a tripod-STIRAP scheme [29]. Here, the polarization of the STIRAP light fields determines which superposition of Zeeman sublevels will be transferred from the $F = 1$ to 2 hyperfine ground level, thus defining the atomic measurement basis.

In our experiment, the STIRAP light field Ω_1 —consisting of a certain superposition of σ^+ and σ^- polarization components—couples an initial superposition of the two Zeeman sublevels of the atomic qubit, i.e., $|1, -1\rangle$ and $|1, +1\rangle$, to the excited state $|F' = 1, m_{F'} = 0\rangle$, and beam Ω_2 couples the excited state to the final hyperfine ground level $|F = 2\rangle$ of the process. The Zeeman sublevel of the final state $|F = 2\rangle$ depends on the polarization of Ω_2 , and is not important for this consideration and, thus, ignored in the further discussion. Regarding the polarization of the light field Ω_1 , a dark

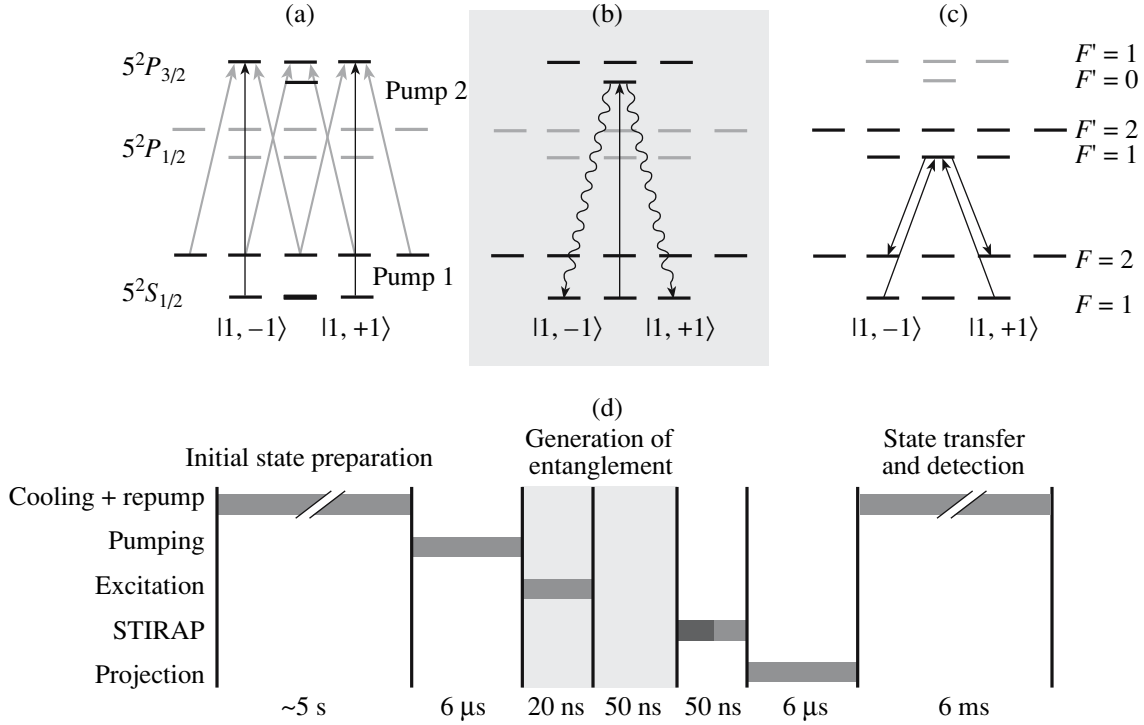


Fig. 5. Sequence for the generation and verification of atom–photon entanglement. (a) Optical pumping resonant to the $F = 1 \rightarrow F' = 1$ and $F = 2 \rightarrow F' = 1$ transitions prepares the atom in the $F = 1, m_F = 0$ ground state. (b) Excitation to the hyperfine level $5^2P_{3/2}, F' = 0$ and subsequent spontaneous decay. The polarization of the emitted photon is entangled with the magnetic sublevel $m_F = \pm 1$ of the $F = 1$ hyperfine level of the atomic ground state. (c) The STIRAP pulse sequence transfers a certain superposition state from the $F = 1$ to the 2 hyperfine level from where the atom is removed from the trap by the projection light field, which induces resonant $F = 2 \rightarrow F' = 3$ transitions (levels omitted for simplicity). Fluorescence of the population left in the $F = 1$ state is used for detection. (d) Timing sequence of the whole process (times not to scale).

state $|\Psi_D\rangle$ and a bright superposition state $|\Psi_B\rangle$, orthogonal to $|\Psi_D\rangle$, exist, given by

$$\begin{aligned} |\Psi_D\rangle &= \cos\alpha|1, -1\rangle + e^{i\phi}\sin\alpha|1, +1\rangle, \\ |\Psi_B\rangle &= \sin\alpha|1, +1\rangle - e^{i\phi}\cos\alpha|1, +1\rangle, \end{aligned} \quad (2)$$

where the angles α and ϕ are defined by the polarization of the STIRAP light field Ω_1 . For example, horizontal linear polarization corresponds to $\alpha = \pi/4$, $\phi = 0$, and, thus, initially couples to the state $|\Psi_B\rangle = (|1, -1\rangle - |1, +1\rangle)/\sqrt{2}$. The state $|\Psi_D\rangle$ is a time-independent dark state that does not couple to the incident light fields at all. On the contrary, the field Ω_1 couples $|\Psi_B\rangle$ to $F' = 1$, and, for slowly time-dependent fields, we obtain a varying $|\Psi_B\rangle$ depending on the angle $\theta(t) = \arctan\Omega_1(t)/\Omega_2(t)$. This results in a coherent adiabatic transfer of $|\Psi_B\rangle$ with a time dependence given by

$$\begin{aligned} |\Psi_B(t)\rangle &= \cos\theta(t)[\sin\alpha|1, -1\rangle - e^{i\phi}\cos\alpha|1, +1\rangle] \\ &\quad - e^{i\phi}\sin\theta(t)|F = 2\rangle, \end{aligned} \quad (3)$$

where ϕ' is the phase difference of the two STIRAP light fields Ω_1 and Ω_2 . The final state of the evolution is $|\Psi_B(\infty)\rangle = |F = 2\rangle$. In essence, the polarization of Ω_1 defines which superposition $|\Psi_B\rangle$ of the states $|1, \pm 1\rangle$ couples to the STIRAP light field and is transferred to the $F = 2$ hyperfine ground level, while the orthogonal superposition state $|\Psi_D\rangle$ remains unchanged and will not be transferred.

The next task is the faithful detection of the two hyperfine ground levels $F = 1$ and 2. A method, widely used to determine the hyperfine level of trapped ions, is the so-called shelving technique [30]. There, the presence or absence, respectively, of resonance fluorescence gives information on the population of the various internal atomic states. In our experiment, shelving cannot be applied. The total detection efficiency for fluorescence photons is 0.1%, and, thus, the atom would have to undergo 20000 excitation emission cycles (without decaying into the other hyperfine ground level), to detect approximately 20 photons that are necessary to distinguish the atomic fluorescence from the background count rates of our detectors. Moreover, the incident shelving light has to be applied along one defined direction. Hence, the scattering of photons

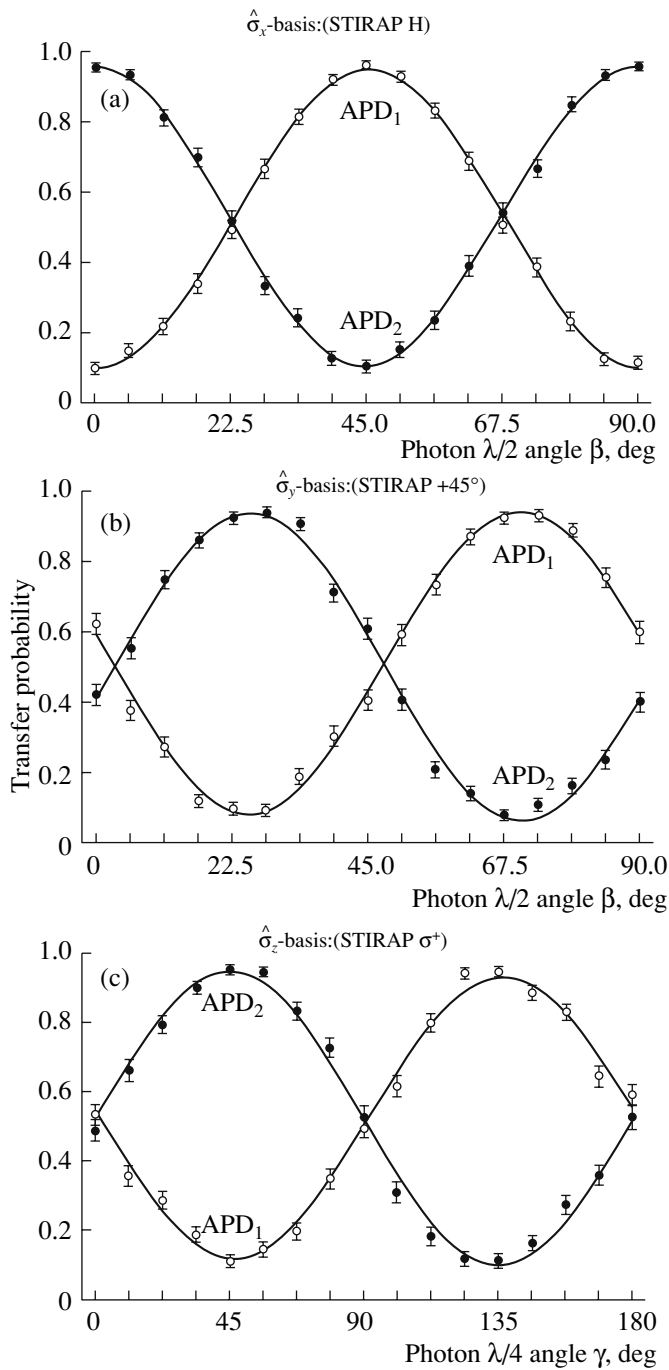


Fig. 6. Atom–photon spin correlations. The figure shows the transfer probability of the STIRAP state analysis as a function of the photon analyzer setting, for an atomic state detection in (a) $\hat{\sigma}_x$, (b) $\hat{\sigma}_y$, and (c) $\hat{\sigma}_z$ basis. The solid lines are sinusoidal fits to the measured data.

gives rise to a radiation pressure force and a heating of the atomic velocity components perpendicular to the direction of the shelving beam.

For the shallow potential of optical dipole traps, this radiation pressure and heating mechanism lead to a loss

of the atom from the trap and definitely renders the shelving method impossible. Instead, we apply a 6- μ s-long circularly polarized projection laser pulse—resonant to the cycling transition—from one direction. An atom in the $F = 2$ hyperfine ground level scatters photons and acquires, on average, one additional photon momentum $\hbar k_{\text{ph}}$ per scattering event. After approximately 50 scattering events, the acquired linear momentum leads to a loss of the atom from the trap. If the MOT beams are then switched on again, fluorescence indicates the atom being in the $|F = 1\rangle$ state and, thus, the projection of the state to the $F = 1$ hyperfine level in the very first scattering process.

Altogether, this method is closely related to employing a polarizing filter for the analysis of polarized light. Compared to the conventional state analysis of single atoms, e.g., developed for ion trap experiments, this method has the clear advantage that no additional manipulations of the atomic qubit state have to be performed. The measurement basis is solely determined by the polarization orientation of the tripod STIRAP, enabling significantly faster and more precise state analysis.

6. ATOM–PHOTON ENTANGLEMENT

Atom–photon entanglement can be prepared by exciting an atom to a state that ideally has two decay channels (Λ configuration). The hyperfine structure of ^{87}Rb offers a good approximation to such a level scheme (Fig. 5b). When excited to the $5^2P_{3/2}$, $F' = 0$ hyperfine level, the atom can spontaneously decay into the three magnetic sublevels $|1, \pm 1\rangle$ and $|1, 0\rangle$ of the $5^2S_{1/2}$, $F = 1$ hyperfine level by emitting a photon at a wavelength of 780 nm. If the emitted photon is left circularly polarized (σ^-), the atom will be in the state $|1, +1\rangle$, whereas we find $|1, -1\rangle$ if the emitted photon is right circularly polarized (σ^+). Since the emitted photons are collected along the quantization axis, π -polarized light (emitted into a different spatial mode) is not collected for symmetry reasons and can be ignored. As long as the σ^\pm emission processes are indistinguishable in all other degrees of freedom, one obtains a coherent superposition of the two decay possibilities, i.e., the maximally entangled state

$$|\Psi\rangle = 1/\sqrt{2}(|1, -1\rangle|\sigma^+\rangle + |1, +1\rangle|\sigma^-\rangle). \quad (4)$$

Here, in each of the terms, the first ket describes the state of the atom, the second one is the polarization of the photon, and the quantum mechanical phase of this superposition follows from the Clebsch–Gordan coefficients of the atomic transitions.

When a single atom is loaded into the trap and its fluorescence is registered, the sequence entangling the atom with a photon is started by pumping it into the $|F = 1, m_F = 0\rangle$ ground state (Fig. 5). Next, a 30-ns optical π pulse excites the atom to the $F' = 0$ level from

which it will decay back to $F = 1$. The emitted photon is detected with an overall efficiency of $\eta_{\text{ph}} \approx 5 \times 10^{-4}$. Thus, the whole excitation and emission process has to be repeated approximately 2000 times which, together with intermediate cooling and trapping cycles, results in an average rate of about 0.2 s^{-1} observed atom–photon couples.

To verify the entanglement of the generated atom–photon state, we perform $\hat{\sigma}_x$, $\hat{\sigma}_y$, as well as $\hat{\sigma}_z$, state analysis of the atomic qubit for different polarization measurements of the photon (Fig. 6, $\hat{\sigma}_i$ are the spin-1/2 Pauli operators). Thereby, the probability of the atom being transferred by the STIRAP pulse sequence, or the probability of remaining in the $F = 1$ ground level, respectively, is measured, conditioned on the polarization measurement outcome of the photon. Varying the photon polarization analyzer, this probability shows the expected sinusoidal dependence. The solid lines in the measurements are sinusoidal fits to the measured data. From the two fits of each measurement, we obtain the visibilities (defined as peak-to-peak amplitude) $V_{\sigma_x} = 0.85 \pm 0.01$, $V_{\sigma_y} = 0.87 \pm 0.01$, and $V_{\sigma_z} = 0.83 \pm 0.01$ for measurement Figs. 6a, 6b, and 6c, respectively. In the $\hat{\sigma}_z$ basis, we observe a significantly smaller visibility. This is due to the higher degree of polarization errors present for this basis, because the atomic and photonic systems are analyzed using circular polarization. Still, all values are clearly above the threshold of 0.72, which clearly proves entanglement of the generated atom–photon state.

7. CONCLUSIONS

Similar to the initial experiments performed with single trapped ions [1], now, also, a single trapped atom allowed us to observe the nonclassical emission of light. Analysis with the second-order correlation function exhibits clear antibunching, proving the single-photon character of fluorescence, and, also, that there is only one atom present at a time in the trap. However, the coherent effects due to a Rabi frequency much higher than the decay rate had now to be described by a four-level scheme, taking into account the levels involved in the MOT fluorescence process. From the spectral characteristics of this single-photon fluorescence, we could determine the temperature of the single atom to be slightly below the Doppler limit.

These measurements laid a firm basis to study the entanglement between the atom and the emitted photon after the decay from the $5 \ ^2P_{3/2}$, $F' = 0$ level. In this (effective) Λ decay, the polarization state of the emitted photon becomes entangled with the magnetic sublevel $m_F = \pm 1$ of the $F = 1$ hyperfine level of the atomic ground state. We adopted coherent STIRAP transfer for the direct analysis of the atomic state, which also enabled state tomography of the combined atom–pho-

ton state [8]. This system is well suited for the interface between an atomic quantum processor and the photonic quantum communication channel [31]. The entanglement achieved in this work is already high enough to enable entanglement swapping, while still maintaining distillable entanglement. It, thus, can be used together with quantum error correction and entanglement distillation for implementing quantum repeaters for long distance quantum communication. Moreover, such entanglement swapping also enables the creation of entanglement between two atoms at quite remote locations. With a distance of about 400 m between the atoms and the nearly perfect detection efficiency of the atoms, a loophole-free test of Bell’s inequality will become possible.

ACKNOWLEDGMENTS

This work was supported by the Deutsche Forschungsgemeinschaft and the European Commission through the EU Project QAP (IST-3-015848).

REFERENCES

1. F. Diedrich and H. Walther, *Phys. Rev. Lett.* **58**, 203 (1987).
2. J. T. Höffges, H. W. Baldauf, W. Lange, and H. Walther, *J. Mod. Opt.* **44**, 1999 (1997); J. T. Höffges, H. W. Baldauf, T. Eichler, et al., *Opt. Commun.* **133**, 170 (1997).
3. G. R. Guthöhrlein, M. Keller, K. Hayasaka, et al., *Nature* **431**, 1075 (2004).
4. N. Schlosser, G. Reymond, I. Protsenko, and P. Grangier, *Nature (London)* **411**, 1024 (2001).
5. J. D. Miller, R. A. Cline, and D. J. Heinzen, *Phys. Rev. A* **47**, R4567 (1993).
6. R. A. Cline, J. D. Miller, M. R. Matthews, and D. J. Heinzen, *Opt. Lett.* **19**, 207 (1994); D. Frese et al., *Phys. Rev. Lett.* **85**, 3777 (2000).
7. K. Saucke, Diploma Thesis (Ludwig-Maximilians Univ., Muenchen, 2002).
8. J. Volz, M. Weber, D. Schlenk, et al., *Phys. Rev. Lett.* **96**, 030404 (2006).
9. D. DiVicenzo, *Fortschr. Phys.* **48**, 771 (2000).
10. N. Schlosser, G. Reymond, and P. Grangier, *Phys. Rev. Lett.* **89**, 023005 (2002).
11. H. J. Carmichael and D. F. Walls, *J. Phys. B* **9**, 1199 (1976).
12. R. Grimm, M. Weidemüllner, and Y. B. Ovchinnikov, *physics/9902072*.
13. C. Monroe, W. Swann, H. Robinson, and C. Wieman, *Phys. Rev. Lett.* **65**, 1571 (1990).
14. S. J. M. Kuppens, K. L. Corwin, K. W. Miller, et al., *Phys. Rev. A* **62**, 013406 (2000).
15. T. Sauter, W. Neuhauser, R. Blatt, and P. E. Toschek, *Phys. Rev. Lett.* **57**, 1696 (1986); J. C. Bergquist, R. G. Hulet, W. M. Itano, and D. J. Wineland, *Phys. Rev. Lett.* **57**, 1699 (1986); W. Nagourney, J. Sandberg, and H. Dehmelt, *Phys. Rev. Lett.* **56**, 2797 (1986).
16. S. Reynaud, *Ann. Phys. (Paris)* **8**, 351 (1983).

17. M. Schubert, I. Siemers, R. Blatt, et al., Phys. Rev. Lett. **68**, 3016 (1992); M. Schubert, I. Siemers, R. Blatt, et al., Phys. Rev. A **52**, 2994 (1995).
18. M. Weber, J. Volz, K. Saucke, et al., Phys. Rev. A **73**, 043406 (2006).
19. M. Lax, Phys. Rev. **145**, 110 (1966).
20. C. Cohen-Tannoudji, J. Dupont-Roc, and G. Grynberg, *Atom-Photon Interactions* (Wiley, New York, 1998).
21. B. M. Garraway and V. G. Minogin, Phys. Rev. A **62**, 043406 (2000).
22. B. R. Mollow, Phys. Rev. **188**, 1969 (1969).
23. F. Schuda, C. R. Stroud, and M. Hercher, J. Phys. B **1**, L198 (1974); F. Y. Wu, R. E. Grove, and S. Ezekiel, Phys. Rev. Lett. **35**, 1426 (1975).
24. W. Hartig, W. Rasmussen, R. Schieder, and H. Walther, Z. Phys. A **278**, 205 (1976).
25. Y. Stalgies, I. Siemers, B. Appasamy, et al., Europhys. Lett. **35**, 259 (1996).
26. H. M. Gibbs and T. N. C. Venkatesan, Opt. Commun. **17**, 87 (1976).
27. C. I. Westbrook et al., Phys. Rev. Lett. **65**, 33 (1990); P. S. Jessen et al., Phys. Rev. Lett. **69**, 49 (1992).
28. J. Oreg, F. T. Hioe, and J. H. Eberly, Phys. Rev. A **29**, 690 (1984); J. R. Kuklinski, U. Gaubatz, et al., Phys. Rev. A **40**, 6741 (1989); G. W. Coulston and K. Bergmann, J. Chem. Phys. **96**, 3467 (1991); T. A. Laine and S. Stenholm, Phys. Rev. A **53**, 2501 (1996).
29. F. Vewinger, M. Heinz, R. G. Fernandez, et al., Phys. Rev. Lett. **91**, 213001 (2003).
30. H. Dehmelt, Bull. Am. Phys. Soc. **20**, 60 (1975).
31. W. Rosenfeld, S. Berner, J. Volz, et al., Phys. Rev. Lett. **98**, 050504 (2007).